

Knowledge Enhanced Conditional Imputation for Healthcare Time-series

Linglong Qian^{1*}, Joseph Arul Raj¹, Hugh Logan Ellis^{1,2},
Ao Zhang³, Yuezhou Zhang¹, Tao Wang¹,
Richard JB Dobson^{1,4,5}, Zina Ibrahim^{1*}

^{1*}Department of Biostatistics and Health Informatics, King's College
London, London, UK.

²Department of Medicine, King's College Hospital NHS Foundation
Trust, London, UK.

³Wellcome Centre for Human Genetics, Nuffield Department of
Medicine, University of Oxford, Oxford, UK.

⁴Institute of Health Informatics, University College London, London, UK.

⁵Health Data Research UK, University College London, London, UK.

*Corresponding author(s). E-mail(s): linglong.qian@kcl.ac.uk;
zina.ibrahim@kcl.ac.uk;

Abstract

We present an end-to-end architecture for managing complex missingness in multivariate time series derived from hospital electronic health records (EHRs). Our Conditional Self-Attention Imputation (CSAI) is a recurrent neural network architecture equipped with a number of techniques aiming to improve imputation accuracy by aligning the model with the subtle temporal and spatial dependencies typical of clinical data. CSAI a) utilises an attention-based hidden state initialisation to capture long- and short-range correlations within the time-series, b) incorporates a knowledge embedding technique to capture clinical data recording patterns and c) employs a non-uniform masking strategy to adapt its weights to the data's temporal and cross-sectional missingness patterns. Extensive evaluation of three EHR benchmark data sets demonstrates that CSAI enhances the current state of the art efficacy in data restoration in addition to performance on downstream tasks. Furthermore, CSAI is integrated within the PyPOTS Python library for benchmarking, offering open and standardised benchmarking capabilities and ease of use for researchers.

Keywords: neural network imputation, healthcare time-series, neural architectures, multivariate time-series imputation, complex missingness

1 Introduction

Multivariate time series obtained from electronic health records (EHRs) play a crucial role in predictive healthcare analytics [1], with many models developed to derive patient-specific insights from EHR data [2, 3]. However, EHR time series are characterised by their complexity, and designing successful downstream predictive models requires addressing the abundance of missingness in correlated variables recorded over time. The nature and timing of the data recorded in EHRs are governed by clinical and administrative decisions, leading to variations in the frequency of documenting vital signs, laboratory tests, and other healthcare measures. For example, heart rate is routinely monitored, while data on white blood cell counts are often scarce, as they are ordered only in specific clinical scenarios, such as suspected infection. In addition, the characteristics typical of EHR data underlie the abundance of correlations between the values and missingness patterns of features over time. For example, because hypertension is a known cause of kidney disease, not only are high blood pressure measurements expected along with abnormal creatinine levels, but EHR datasets generally show high correlations between the recording patterns of blood pressure and urine creatinine levels [4]. The inherent irregularities render more than 50% of EHR data missing not at random [5], with significant variations in missingness patterns between tasks and datasets [5]. These challenges create a complex landscape for imputation algorithms [6–9] and highlight the importance of domain knowledge in modelling accuracy.

Recent advances in deep learning have shown significant potential in addressing the complexities of EHR missingness. In particular, models based on Recurrent Neural Networks (RNNs), such as GRU-D [10], BRITS [11], and M-RNN [12], have proven effective in capturing EHR temporal and cross-sectional dependencies. Among these, BRITS has shown superior performance in datasets of varying characteristics [13, 14]. BRITS uses bi-directional RNN dynamics and treats missing data as variables of the bidirectional RNN graph, subsequently involving them in the backpropagation process. Using this strategy, missing values accumulate gradients in both forward and backward directions with consistency constraints, increasing the accuracy of estimated values.

Despite advances, none of the existing models, including BRITS, account for domain-imposed disparities in feature-recording patterns, which can have critical implications on imputation accuracy. We show that incorporating a domain-informed strategy to capture feature correlations is particularly suited for our domain. In addition, the temporal correlations in the EHR data can span both short- and long-term intervals. For example, while monitoring diabetic patients, both short-term glucose fluctuations and long-term HbA1c levels must be accurately modelled, while cardiovascular risk assessment requires careful cross-sectional examination of biomarkers like cholesterol, glucose, and blood pressure. Although RNNs excel at capturing short-term temporal dependencies in a time series, they are less capable of capturing long-range

correlations over time [7]. Finally, all current models rely on random masking as a pre-processing step to generate ground truths for evaluation purposes. This involves designating a randomly selected subset of complete values as missing, primarily creating missing completely at random (MCAR) scenarios and drastically oversimplifying the temporal and cross-sectional dependencies in real EHR time series.

To address these issues, we developed CSAI, a bi-directional RNN using BRITS as a backbone to support a transformer-based attention mechanism for hidden state initialisation and propagation. CSAI extends BRITS to better suit the characteristics of EHR data through the following contributions:

1. Improved initialisation of hidden states to more effectively model temporal dynamics between data points. Our conditional hidden state initialisation leverages self-attention to account for long-term dynamics, complementing those already captured by the RNN and propagating them through the hidden states, thereby improving overall performance.
2. We present a domain-informed *temporal decay* function that determines the likelihood of missing values being linked to past observations based on clinical recording patterns in the dataset. The decay of a feature is used to adjust its associated attention mechanism, enabling a more fine-grained, feature-specific representation of temporal relationships within the data.
3. CSAI is integrated with a non-uniform masking strategy to selectively mask data in a way that reflects the inherent structured patterns of interdependencies within the dataset across time and features.

The missing data patterns in the EHR reflect the underlying data structures and convey clinically relevant information about the variables used in the analysis tasks. Aligning the imputation process with these characteristics can significantly impact the quality of downstream predictive models. CSAI’s contributions mark an important step toward enhancing imputation algorithms to better capture domain-specific patterns in EHR data, leading to improved performance in tasks like patient prognosis and clinical decision-making.

2 Related Work

The ability of RNNs to capture temporal evolution has made them an attractive choice for time-series imputation. The GRU-D model [10] introduced the use of temporal decay to recurrent imputation models, whereby the influence of past recordings on missing data decreases over time, with features imputed closer to default values if their last observation occurred a long time ago. Using this concept, GRU-D estimates missing values through a combination of the last recorded value and the global mean within a recurrent architecture. Although this approach alone has shown impressive performance in certain healthcare applications, its effectiveness has not been generalisable in other datasets [11], particularly in accounting for discrepancies in vital signs recording frequencies and laboratory tests.

Several extensions of GRU-D exist. M-RNN [12] and BRITS [11] use bi-directional RNNs to capture temporal dynamics in both forward and backward directions, improving imputation accuracy. Both M-RNN and BRITS combine RNNs with a feed-forward component to capture additional correlations across features. However, M-RNN treats imputed values as fixed constants while BRITS treats missing values as variables, updating them through backpropagation and demonstrating superior performance across various domains [13, 15].

Transformers have shown strong performance in capturing long-term dependencies through their self-attention mechanism [16] and have been used to model missingness at random in SAITS [17]. However, Transformers face challenges in capturing short-term dynamics in time series data and their effectiveness in handling fine-grained temporal details and complex missing patterns remains debatable [16]. Models like NRTSI [18], though designed to handle these issues, struggle with computational complexity [17].

Some imputation efforts prioritise the ability to quantify one’s confidence in the resulting imputation, introducing stochasticity into their architectures. This includes RNN-based models such as GRU-U [19], variational autoencoders such as V-RIN [20], generative adversarial networks such as E^2 GAN [21] and diffusion models as in CSDI [22]. Apart from CSDI, all these approaches require additional stochastic modules added to the imputing network, resulting in unstable training due to increased coupling, and ultimately leading to less accurate imputation in comparative studies [23]. Although CSDI [22] successfully exploits the correlations between observed values to measure stochasticity, it suffers from data leakage as indicated in its repository.

CSAI aims to build on the current state of neural network imputation by addressing unsolved challenges. By encoding transformer-based self-attention to a bi-directional RNN architecture, CSAI captures long-term dependencies which may be missed by BRITS and similar RNN-based models [11]. Furthermore, introducing the domain-informed temporal decay function refines the imputation process beyond standard decay techniques [10]. Finally, integrating CSAI with a non-uniform masking strategy specifically targets the complex temporal and cross-sectional relationships in EHRs.

3 Terminology and Background

3.1 Incomplete Multivariate Time-series Representation

For a temporal observation over T discrete time steps, we represent a multivariate time series as a matrix $\mathbf{X} \in \mathbb{R}^{T \times D}$. $\mathbf{X} = \{\mathbf{x}_1, \mathbf{x}_2, \dots, \mathbf{x}_T\}$ is composed of T observations, each denoted by a vector $\mathbf{x}_t \in \mathbb{R}^{1 \times D}$ of D features observed at timestamp s_t .

Information related to missing values is encapsulated within two derived matrices (see Fig.1). The mask matrix $\mathbf{M} \in \mathbb{R}^{T \times D}$ indicates whether each element of \mathbf{X} is observed or missing:

$$m_t^d = \begin{cases} 0, & \text{if } x_t^d \text{ is missing} \\ 1, & \text{otherwise} \end{cases} \quad (1)$$

Furthermore, given that the time elapsed between consecutive observations can vary, we denote the time gaps at each time step by an additional component δ_t^d .

$\delta_t^d \in \mathbb{R}^{T \times D}$ encodes the time gap between two successive observed values for each feature d , providing an additional indicator of temporal context to the dataset.

$$\delta_t^d = \begin{cases} s_t - s_{t-1} + \delta_{t-1}^d & \text{if } t > 1, m_t^d = 0 \\ s_t - s_{t-1} & \text{if } t > 1, m_t^d = 1 \\ 0 & \text{if } t = 1 \end{cases} \quad (2)$$

Time series \mathbf{X}					Mask					Time gap					
5	/	/	8	9	1	0	0	1	1	0	4	5	7	2	$d = 1$
7	/	/	/	9	1	0	0	0	1	0	4	5	7	9	$d = 2$
2	4	1	6	/	1	1	1	1	0	0	4	1	2	4	$d = 3$
x_1	x_2	x_3	x_4	x_5	m_1	m_2	m_3	m_4	m_5	δ_1	δ_2	δ_3	δ_4	δ_5	

Fig. 1: An example of multivariate time-series. Observations \mathbf{x}_{1-5} in time-stamps $s_{1-5} = 0, 4, 5, 7, 9$. Feature d_2 was missing during s_{2-4} , the last observation took place at s_1 . Hence, $\delta_5^2 = t_5 - t_1 = 9 - 0 = 9$.

3.2 Overview of the BRITS Backbone

BRITS exploits cross-sectional and temporal correlations in multivariate time series through two dedicated components, a fully connected regression module and a recurrent module, respectively. It also relies on the notion of temporal decay (Eq.(4)) to capture temporal correlations and adjust their influence on missing values based on temporal distance. The BRITS architecture accepts a time series \mathbf{X} , such that missing values within an observation $\mathbf{x}_t \in \mathbf{X}$ are managed via a corresponding masking vector \mathbf{m}_t and a time gap vector δ_t as shown at the bottom of Fig.2.

Because an observation \mathbf{x}_t may contain missing values, it cannot be directly ingested by the two BRITS components. Instead, BRITS uses the notion of *decay* to derive estimates for missing cells. Temporal decay dictates that the strengths of the correlations are inversely related to the time-gap δ_t and is formalised by the decay factor $\gamma_t \in (0, 1]$ (Eq.(4)). In the equation, \mathbf{W}_γ and \mathbf{b}_γ are parameters. The calculated decay factor γ_t for the hidden state is then used to transform \mathbf{h}_{t-1} to the *decayed* hidden state, $\hat{\mathbf{h}}_{t-1}$ as in Eq.(5). BRITS uses the decayed hidden state to find the historical estimation $\hat{\mathbf{x}}_t$, of \mathbf{x}_t as in Eq.(6). Using masking vector \mathbf{m}_t obtained from \mathbf{M} , $\hat{\mathbf{x}}_t$ is then used to replace the missing values of \mathbf{x}_t , yielding the *complement vector* \mathbf{x}_t^h , which embeds temporal missingness patterns to be fed into subsequent BRITS components (Eq.(7)).

$$\mathbf{h}_0 = 0 \quad (3)$$

$$\gamma_{th} = \exp(-\max(0, \mathbf{W}_\gamma \delta_t + \mathbf{b}_\gamma)) \quad (4)$$

$$\hat{h}_{t-1} = h_{t-1} \odot \gamma_t \quad (5)$$

$$\hat{x}_t = W_x \hat{h}_{t-1} + b_x \quad (6)$$

$$x_t^h = m_t \odot x_t + (1 - m_t) \odot \hat{x}_t \quad (7)$$

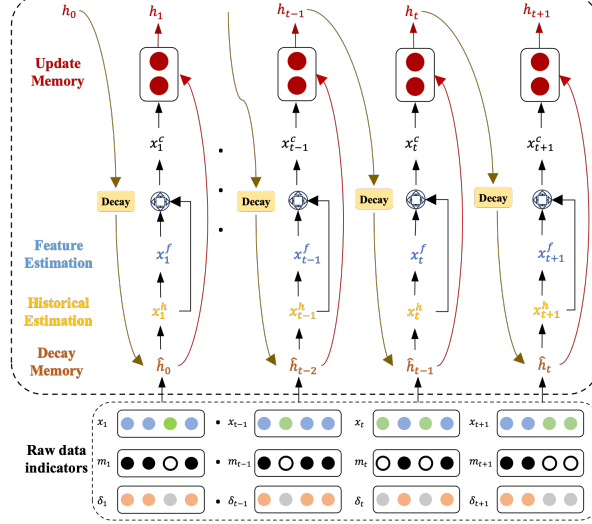


Fig. 2: The BRITS backbone processes

BRITS explores cross-sectional correlations within a single observation through a fully connected layer, generating x_t^f , a feature-wise approximation of missing values (Eq.(8)). The concept of decay extends to the feature space, resulting in a learnable factor $\hat{\beta}_t$, taking into account the temporal decay and the masking vector (Eq.(9)-(10)). This integration produces the imputed matrix x_t^c , effectively combining observed and imputed data (Eq.(11)-(12)).

$$x_t^f = W_z x_t^h + b_z \quad (8)$$

$$\gamma_{tf} = \exp(-\max(0, W_{\gamma f} \delta_t + b_{\gamma f})) \quad (9)$$

$$\hat{\beta}_t = \sigma(W_\beta [\gamma_{tf} \circ m_t] + b_\beta) \quad (10)$$

$$\hat{x}_t^c = \hat{\beta}_t \odot x_t^f + (1 - \hat{\beta}_t) \odot x_t^h \quad (11)$$

$$x_t^c = m_t \odot x_t + (1 - m_t) \odot \hat{x}_t^c \quad (12)$$

$$h_t = \sigma(W_t \hat{h}_{t-1} + U_h [x_t^c \circ m_t] + b_h) \quad (13)$$

The final step of BRITS (Eq.(13)) updates the hidden state via its RNN component, leveraging various indicators to learn functions of past observations. Bidirectional recurrent dynamics is used to address slow convergence by using information in the backward direction.

The entire process is shown in Fig.2. BRITS bidirectional architecture combined with its decay mechanism represents a significant advancement for multivariate time series imputation, addressing the challenge of temporal correlations at a level of sophistication unmatched by traditional methods.

4 Methodology

In this section, we describe the modifications proposed to the BRITS architecture to incorporate a) a domain-informed temporal decay functionality, and b) the ability to capture long-range correlations via a transformer-based conditional hidden state initialisation. In addition, we describe a novel non-uniform masking strategy to explicitly model non-random missingness.

4.1 Domain-informed Temporal Decay

The BRITS decay function Eq.(4) is strictly dependent on temporal proximity, dynamically adjusting the contribution of a past observation to a missing value based on the length of the time gap between the two. Although this decay mechanism effectively captures the intuition that more recent observations carry greater diagnostic value, it overlooks the discrepancies in the clinical recording patterns of different features. This can be illustrated in the example below.

Example 1. Let features f_1 and f_2 be two features representing heart rate (HR) and systolic blood pressure (SBP) respectively; HR is typically recorded more frequently than SBP. BRITS is presented with an observation \mathbf{x}_t with missing HR and SBP values. The time gap vector shows $\delta_t^{f_1} = 2$ and $\delta_t^{f_2} = 7$. According to the principle of temporal decay, BRITS will ignore the typical recording patterns of the two features and the last observation for f_2 will incorrectly have less weight on the imputed value than that of f_1 .

Our new decay mechanism prioritises recent observations while accounting for the natural variability in healthcare data collection. In addition to using the observed time gap δ_t^d , we modify the decay function to incorporate the expected time gap τ between two recordings of a given feature. τ for a feature is the overall median of all gap lengths between any two consecutive feature recordings in the dataset. The adjusted decay function only reduces the weight assigned to an observation if its last observed value lies outside τ and allocates more weight to observations closer to the expected time gap and less to those further away, as given below:

$$A_t = \exp(-\max(0, \mathbf{W}_\gamma(\delta_t - \tau) + \mathbf{b}_\gamma)) \quad (14)$$

This ensures that the attention peaks when the time gap δ_t closely matches τ , and declines as the difference between δ_t and τ increases.

Example 2. For the same features f_1 and f_2 , examining the dataset shows that the median time gaps for the two features are $\tau_1 = 2$ for HR, compared to $\tau_2 = 10$ for SBP respectively. These medians reflect the fact that HR is much more frequently monitored than SBP in routine clinical practice. Here, because the past recordings fall within the respective time gaps for both features, the past values will be assigned equal weights to

the missing values. In this way, the less frequently measured SBP (with a median gap of 10) is not unfairly penalised.

4.2 Hidden State Initialisation

The hidden state of the recurrent component of BRITS are not generated through the raw input. Instead, they receive incomplete data with missingness indicators for imputation, i.e. $\hat{\mathbf{h}}$ replaces \mathbf{h} in Eq.(5). However, the hidden states in BRITS are initialised with zeros. Since information decay starts at the first step, zeros \mathbf{h}_0 will cause \mathbf{x}_1^h and \mathbf{x}_1^f fully rely on neural network parameters, then accumulate.

Instead, our approach makes use of the last observed data point and a decay attention mechanism to generate a conditional hidden state distribution $q(\mathbf{h}_{\text{init}}|\mathbf{x}_{\text{last_obs}}, \mathbf{A}(\delta_t, \tau))$ within the model distribution $p_\theta(\mathbf{x}_t)$. This strategy is designed to provide a more contextually rich starting point for the model, thus enhancing the effectiveness of subsequent imputations. In addition, unlike in BRITS where the decay factor is applied directly to the previous hidden state Eq.(5) and Eq.(9), our approach uses the decay factor to modulate the attention mechanism. This modification allows for a more fine-grained and feature-specific generation of temporal relationships within the data, enhancing the model ability to adapt to varying temporal dynamics across different features. Our approach is described in detail below.

Input projection and positional encoding. At each time step \mathbf{s}_t , the last observation $\mathbf{x}_{\text{last_obs}} \in \mathbb{R}^{T \times D_{\text{feature}}}$ from input time-series data \mathbf{x}_t undergo transformation alone with $\mathbf{A}(\delta_t, \tau) \in \mathbb{R}^{T \times D_{\text{feature}}}$ from Eq.(14). The Positional Encoding module and an Input Projection module are used to transform them into $\mathbb{R}^{T \times D_{\text{model}}}$, defined as:

$$\mathbf{x}'_{\text{last_obs}} = \text{PosEncoder}(\text{InputProj}(\mathbf{x}_{\text{last_obs}})) \quad (15)$$

$$\mathbf{A}'(\delta_t, \tau) = \text{PosEncoder}(\text{InputProj}(\mathbf{A}(\delta_t, \tau))) \quad (16)$$

Transformer enhancement. The concatenated input for the Transformer Encoder \mathbf{C}_{in} is formed by combining transformed last observation and decay attention and processed through multiheaded self-attention (MSA), layernorm (LN), and feed-forward networks (FFN).

$$\mathbf{C}_{\text{in}} = \text{Concat}(\mathbf{x}'_{\text{last_obs}}, \mathbf{A}'(\delta_t, \tau)) \quad (17)$$

$$\mathbf{C}_{\text{out}} = \text{LN}(\text{FFN}(\text{LN}(\text{MSA}(\mathbf{C}_{\text{in}})))) \quad (18)$$

Information scaling to initialise hidden state. The enhanced output of the transformer Encoder is scaled to the dimensions required by the hidden state \mathbf{h}_{init} through alternating 1D convolution.

$$\mathbf{H}_1 = \text{Conv1D}_1(\mathbf{C}_{\text{out}}\mathbf{W}_1 + \mathbf{b}_1) \quad (19)$$

$$\mathbf{h}_{\text{init}} = \text{Conv1D}_2(\mathbf{H}_1\mathbf{W}_2 + \mathbf{b}_2) \quad (20)$$

where Eq.(19) transform C_{out} from $\mathbb{R}^{2L \times d_{\text{model}}}$ to $\mathbb{R}^{2L \times d_{\text{hidden}}}$ and produces H_1 , Eq.(20) further scale H_1 to generate the initialized Hidden State h_{init} . The CSAI architecture is shown in Fig.3.

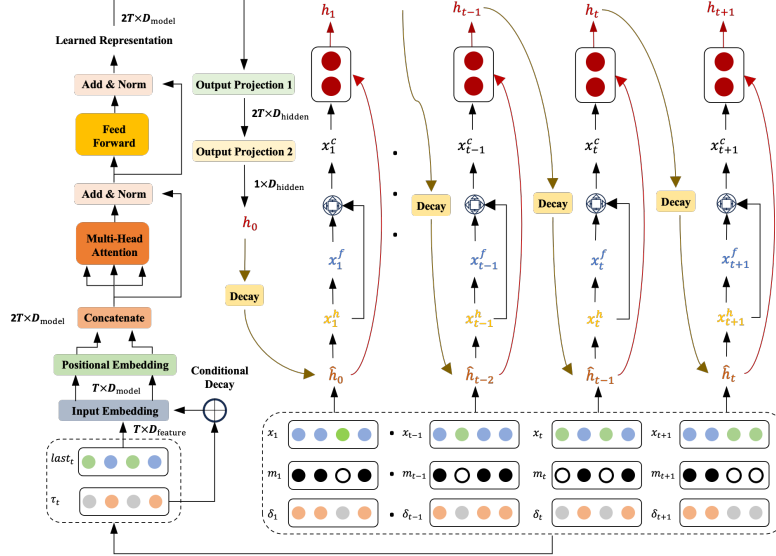


Fig. 3: The CSAI architecture, which equips BRITS with self-attention. CSAI begins with an input embedding layer, transforming raw data into a dense representation. Positional embedding is applied next, adding temporal context to the input, enabling the model to capture time dependencies. These embeddings are concatenated to form a unified input that integrates the data’s temporal structure. The input is then processed through multi-head attention, normalisation, and feed-forward layers, with decay attention mechanisms modulating the importance of previous observations. The final output is used to initialise hidden states for subsequent recurrent layers, accounting for both temporal dynamics and domain-specific variability in recording patterns.

4.3 Non-Uniform Masking Strategy

Our non-uniform masking strategy fundamentally diverges from traditional approaches by leveraging the inherent missingness distribution. This strategy is predicated on the principle outlined in the introduction, whereby the probability of missingness in healthcare data is not uniformly distributed across features. Instead, it varies according to healthcare practices and patient conditions. By incorporating this variability into our masking process, we aim to create a more realistic and representative model of the missing data patterns.

The core of our algorithm involves generating non-uniform masking probabilities guided by the missingness distributions of each feature. Another essential aspect is the manual adjustment factor, designed to fine-tune the masking process. This factor is

adaptively set based on the observation frequency per feature, allowing for a tailored masking strategy. This adaptive approach aims to achieve a balance between avoiding overfitting in sparse data scenarios and ensuring sufficient learning signals in data-rich contexts. It is designed to optimise the model’s ability to discern underlying patterns and relationships, enhancing its predictive accuracy and generalisation across diverse healthcare data patterns. For a given feature d , the non-uniform masking probability $\mathbf{P}_{\text{nu}}(d)$ is determined as follows:

$$\mathbf{R}_{\text{factor}}(d|U, I) = \mathbf{F}(d, U, I) \quad (21)$$

$$\mathbf{P}_{\text{nu}}(d) = \mathbf{R}_{\text{factor}}(d|U, I) \times \mathbf{P}_{\text{dist}}(d) \quad (22)$$

Where:

- U and I are the pre-defined parameters. U is the masking rate, i.e. the percentage of the ground truths masked during training. I is a weighting parameter.
- $\mathbf{R}_{\text{factor}}(d|U, I)$ is the regulatory factor for feature d , conditioned by U and I .
- $\mathbf{P}_{\text{dist}}(d)$ represents the probability distribution of missingness for feature d .

The overall masking proportion is then adjusted to ensure consistency with the uniform masking rate U , while retaining the non-uniform characteristics of the individual features. The pseudocode for this algorithm is as follows:

Algorithm 1 Non-Uniform Masking Strategy

Input: Dataset \mathbf{X} with D features, Uniform masking rate U , weighting parameter I
Output: Masked Dataset \mathbf{X}_M
for feature d in D **do**
 $\mathbf{P}_{\text{dist}}(d) \leftarrow \mathbf{x}^d$
 $\mathbf{R}_{\text{factor}}(d) \leftarrow f(U, I)$
 $\mathbf{P}_{\text{nu}}(d) \leftarrow \mathbf{R}_{\text{factor}}(d) \times \mathbf{P}_{\text{dist}}(d)$
end for
 $U \leftarrow f(\mathbf{P}_{\text{nu}}(d), \mathbf{x}^d)$
 $\mathbf{X}_M \leftarrow \mathbf{P}_{\text{nu}} \times \mathbf{X}$

5 Experimental Evaluation

We conducted a number of experiments to evaluate the proposed methodologies and their effect on CSAI’s performance. First, we compared CSAI’s overall imputation and classification performance against five state-of-the-art baselines using four real-world healthcare datasets. The comparison includes BRITS, BRITS with GRU (BRITS-GRU), GRU-D, V-RIN, and M-RNN. We included BRITS-GRU alongside the original BRITS, which uses LSTM cells, to ensure a fair comparison, as the other baselines employ GRU cells. This addition allows for a more comprehensive and balanced evaluation across similar architectures. Although a comparison with E^2 GAN would have provided valuable insight, particularly given its lack of quantitative comparison with BRITS, the publicly available implementation of E^2 GAN is incompatible with our

current setup. To ensure reproducibility of our results, all data preprocessing scripts, model implementations, and hyperparameter search configurations are released.

We then perform a two-fold ablation study using the openly-available Physionet dataset to evaluate the merit of the proposed non-uniform masking strategy. First, our study establishes the effect of non-uniform masking across different data partitions, namely the training, validation and test sets. The aim is to establish whether this approach indeed improves a model’s ability to generalise and handle missing data in a more realistic and robust manner. Finally, we evaluate the effect of the weighting parameter, which controls the degree of emphasis placed on different features in the non-uniform masking strategy. This parameter allows for fine-tuning of the feature representation during model training, directly influencing how the model handles missing data. This set of experiments evaluates the effect on CSAI’s imputation and classification performance under varied the weighting parameter values.

5.1 Datasets

Each of the four datasets chosen for the experimental evaluation has a different data distribution, especially the MIMIC-III database, from which we extracted two different datasets to model different tasks. We reproduced the benchmarking for these public datasets, skipping steps that remove all-NAN samples to retain the data with its original missingness.

1. **eICU**¹ [24] is sampled from the eICU Collaborative Research Database, a multi-center database with anonymised hospital patient records. eICU is publicly available after registration, including completion of a training course in research with human subjects and signing of a responsible data use agreement. We followed the only benchmarking extract available for eICU [25], yielding a dataset comprising 30,680 samples measuring 20 features, 3 of which were categorical.
2. **MIMIC-III**² [26] is an extensive, freely-available database of over 40,000 critical care patients. To complement our MIMIC experiments with heterogeneous feature types and data dimensionality, we followed two benchmark papers [27, 28] to produce two datasets. The first comprises 89 (10 of which are categorical) variables for 14,188 samples while the second captures 59 numerical variables for 21,128 samples.
3. **PhysioNet Challenge 2012 dataset.** The Predicting Mortality of ICU Patients: The PhysioNet/Computing in Cardiology Challenge 2012, a public medical benchmarking dataset provided by [29], contains records of 4000 48-hour ICU stays, allowing unbiased evaluations of different model performances. This benchmark comprises 35 numerical variables for 3,997 samples.

5.2 Implementation Details

We trained our models on an HPC node with NVIDIA A100 40GB running Ubuntu 20.04.6 LTS (Focal Fossa). We used Python: 3.8.16. All package details can be found in our repository. For each of the five datasets, we created three versions by further masking 5%, 10% and 20% cells in addition to the missingness already present in the

¹<https://physionet.org/content/eicu-crd/2.0/>

²<https://physionet.org/content/mimiciii/1.4/>

original datasets. These masked cells have known ground truths and will form the basis of our comparison of imputation performance.

We used the Adam optimiser and set the number of RNN hidden units to 108 for all models. The batch size is 64 for PhysioNet and 128 for the other datasets. Each dataset was normalised to zero mean and unit variance. Randomly, we selected 10% of each dataset for validation and another 10% for testing, training the models on the remaining data. For the imputation task, we masked 10% of observations in each dataset to serve as the ground truth, which was used as validation data. A 5-fold cross-validation method was implemented to evaluate the models. Imputation and classification performance was measured using the Mean Absolute Error (MAE) and Area Under the Receiver-Operator Curve (AUC-ROC) respectively. We adopted a non-uniform masking strategy for the training set in all datasets. The code for CSAI is available on GitHub: <https://github.com/LINGLONGQIAN/CSAI>.

5.3 Experimental Results

Comparison with State-of-the-Art Models. Our evaluation of CSAI against five state-of-the-art models using four diverse healthcare data sets is shown in Tables 1 and 2. Table 1 shows imputation performance, where CSAI consistently achieved the lowest MAE compared to all other models. This is particularly evident in lower masking ratios on both the eICU and mimic_59f datasets, suggesting that CSAI effectively uses its conditional knowledge embedding under limited data conditions to accurately impute missing values.

Table 1: Imputation performance using 5%, 10% and 20% masking ratios on the four datasets. In each setup, the model with the highest MAE is highlighted in bold.

	eICU (MAE)			MIMIC_59f (MAE)		
	5	10	20	5	10	20
BVRIN	0.2416066624555	0.2425388767962	0.2521443794081	0.15457482983029	0.1381774096223	0.3369691066028
BRITS	0.1669909016914	0.1705338793299	0.1768130684914	0.1519486919982	0.1402299219611	0.3403944741631
BRITS_GRU	0.172319898527	0.1712448395078	0.1769143760391	0.1479284907740	0.1419320843095	0.3416945429830
GRUD	0.2227370102738	0.2256000191395	0.2309779583607	0.3044727329354	0.2870424025309	0.4866963332628
MRNN	0.4703575678949	0.4799816897156	0.5006539067069	0.305728740144	0.2834192980232	0.4719812224131
CSAI	0.1596681888527	0.1614887556508	0.1663724494172	0.1311938059021	0.1129106347724	0.3097617904199
	PhysioNet (MAE)			MIMIC_89f (MAE)		
	5	10	20	5	10	20
BVRIN	0.261627214279	0.2737156899792	0.2999655482813	0.2802916356976	0.2981212480367	0.3249882376070
BRITS	0.2563447937357	0.2676201849977	0.2872153778145	0.2846978765928	0.3063578035340	0.3298037475677
BRITS_GRU	0.2512872199774	0.2621551395257	0.2828820523984	0.2833476046520	0.3020169393225	0.325679723132
GRUD	0.4940628434272	0.4977919324802	0.509515400807	2.162001471223	2.226354328684	2.300878604115
MRNN	0.5467116967567	0.5564676306450	0.5722952103217	0.5077789122169	0.5202164923417	0.5340895067570
CSAI	0.2460182594695	0.2574714476838	0.2747586037341	0.2845187575872	0.2984590455884	0.3277731324925

Table 2 further demonstrates CSAI’s strong classification performance, achieving competitive AUC scores across various masking ratios in the eICU, PhysioNet, and MIMIC_59f datasets. However, CSAI slightly underperforms in the MIMIC_89f compared to BRITS-GRU. Notably, this dataset contains a high proportion of categorical variables, for which the architectural modifications of CSAI may not be as advantageous and which highlights the need for further tuning. Nevertheless, the robustness of the BRITS architecture further validates its selection as the CSAI backbone.

Table 2: Classification performance using 5%, 10% and 20% masking ratios on the four datasets. In each setup, the model with the highest AUC is highlighted in bold.

	eICU (AUC)			MIMIC.59f (AUC)		
	5	10	20	5	10	20
	BVRIN	0.8876632792674	0.8842207935257	0.8846083295889	0.8327985224797	0.8331225972961
BRITS	0.8866858256973	0.8852105575201	0.8856887012643	0.8282097938406	0.8277898698471	0.8241398505926
BRITS_GRU	0.8894446123008	0.8866442109252	0.8860531724480	0.8318754575867	0.830741815613	0.826876535038
GRUD	0.8649508677163	0.8645586279780	0.8580064406861	0.8276771341543	0.8263960525470	0.8230358085344
MRNN	0.8778555135764	0.8762569153075	0.8734187899382	0.8210628460196	0.8170771816893	0.8128184260363
CSAI	0.8895208094995	0.8897650378954	0.8879479677632	0.8352381478170	0.8336724124061	0.8310903756879
	PhysioNet (AUC)			MIMIC.89f (AUC)		
	5	10	20	5	10	20
	BVRIN	0.8343250745783	0.8291631265561	0.8254836447961	0.8515838497027	0.8483391172226
BRITS	0.822140767045	0.811750067602	0.8218051204357	0.8518059085347	0.8499103429115	0.8410220558148
BRITS_GRU	0.8067688302396	0.8192578961191	0.8065060341956	0.85410308259	0.852057183334	0.84306840205
GRUD	0.789974428059	0.7765171413166	0.7698864925325	0.7924280641870	0.789628259467	0.7732159684544
MRNN	0.8012121900939	0.7994518346619	0.7939973744164	0.828283355107	0.8303854640068	0.823715692404
CSAI	0.86464530892	0.85919145690	0.83722349351	0.837759164790	0.8400507785337	0.8317807876933

Evaluating Non-uniform Masking. The effect of different configurations on model performance was evaluated by non-uniformly masking various combinations of the training, validation, and test sets, while examining the number of training epochs required to achieve the reported performance for each. The results for the BRITS and BRITS-GRU baseline models are shown in Table 3. These results demonstrate that consistently applying non-uniform masking across all data partitions yielded the best performance. This suggests that the masking strategy effectively adjusts the representation of different features to optimally leverage the data’s distribution, enhancing the model’s ability to handle the inherent heterogeneity of the dataset.

Weighting Parameter Comparison. The non-uniform masking probability for a given feature is determined the parameters U and I , in addition to the feature’s prior probability as shown in Eq.(21)- (22). Having examined CSAI’s performance with different masking ratios (i.e U values) in Section 5.3, we now study the effect of the weighting parameter I on the resulting imputation and classification performance. The findings are shown in Table 4 and are further illustrated in Fig.4. An optimal weighting parameter, shown to be around 5, results in the lowest imputation error, suggesting that a balanced representation of features is crucial for accuracy. However, for classification, increasing the weighting parameter leads to higher errors and a marginal decrease in the AUC, highlighting that excessive weighting may not uniformly improve performance across different machine learning tasks. These findings reveal the interplay between feature representation adjustments and task-specific model efficacy, underscoring the importance of calibration in the non-uniform masking approach for complex time series data.

6 Discussion and Conclusions

This study introduced CSAI, a novel approach for imputing and classifying missing data in multivariate medical time series. CSAI demonstrated significant potential to improve the accuracy and reliability of medical data analysis, which is critical for high-stakes healthcare decision making. Using conditional knowledge embedding and

Table 3: Performance comparison across masking permutations showing the impact of different non-uniform masking strategies on both imputation and classification, using the BRITS and BRITS-GRU models. **Train only:** Non-uniform masking applied solely to the training set. **All:** non-uniform masking is applied across all training, validation and test sets. **None:** a baseline with no non-uniform masking. **Val only:** Non-uniform masking is applied only to the validation set. **Val Test:** Non-uniform masking is applied to both the validation and test sets. **Test only:** Non-uniform masking is applied exclusively to the test set. Under the 'All' configuration, non-uniform masking is applied during training, validation, and testing consistently demonstrates superior performance (bold font).

Model	Masking	Imputation		Classification		
		Epoch	MAE	Epoch	MAE	AUC
Brits	All	182.2	0.234929	28.6	0.262997	0.819142*
	Val_Test	187	0.235739	57	0.262268	0.816184
	Test_only	218.6	0.236001	61.6	0.265496	0.813821
	Train_only	215.8	0.266307	25.4	0.310624	0.815686
	None	218.6	0.26762	61.6	0.313257	0.81175
	Val_only	187	0.268386	57	0.309332	0.818605
Brits-GRU	All	294.8	0.231594	21.8	0.26615	0.821869*
	Val_Test	287.4	0.233243	21.6	0.267872	0.813855
	Test_only	286	0.23363	15.4	0.270678	0.811355
	Train_only	288.4	0.258989	17.6	0.313681	0.815697
	Val_only	287.4	0.262149	21.6	0.314871	0.81071
	None	286	0.262155	15.4	0.318493	0.819258

Table 4: Impact of weighting parameter I on imputation and classification performance metrics. The table showcases the number of epochs required, imputation MAE and classification AUC across varying weighting factors.

I	Imputation		Classification		
	Epoch	MAE	Epoch	MAE	AUC
0	286	0.26215514	15.4	0.31849296	0.8192579
5	291.2	0.2310647	33.8	0.26586726	0.80975966
10	294.8	0.23159396	21.8	0.26615049	0.8118691
50	293	0.24170042	16.4	0.28670924	0.81583396
100	285.8	0.26885496	14.2	0.32437366	0.81381879
150	283.8	0.29943347	16.6	0.35346112	0.8144707
200	289.2	0.33235399	15.6	0.39360851	0.81173828

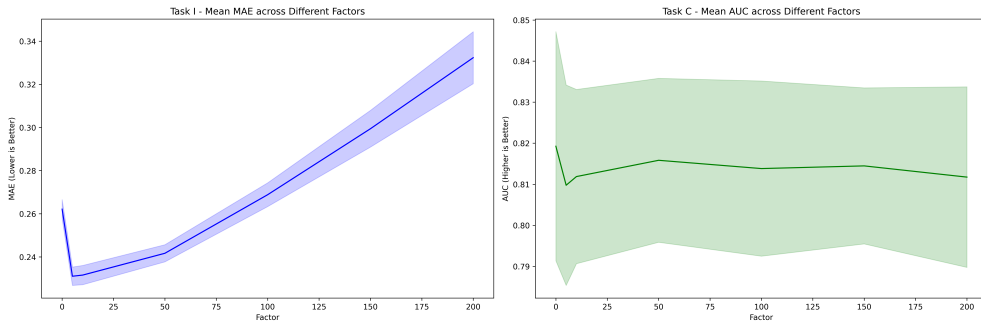


Fig. 4: Impact of Adjustment Factor on Model Performance in the Physionet Dataset.

attention mechanisms, CSAI outperformed established benchmarks in multiple real-world healthcare datasets, particularly in scenarios with lower masking ratios. Its ability to model non-random missingness and capture complex temporal relationships positions it as a valuable tool for real-world clinical applications.

Our comprehensive experimental evaluation showcased the efficacy of CSAI in diverse healthcare datasets, where it frequently surpassed baseline state-of-the-art models such as BRITS, BRITS-GRU, and others. CSAI consistently achieved the lowest imputation error and competitive classification performance in various masking configurations. The strong results suggest that CSAI can be instrumental in providing a strong base for predictive models used in various downstream tasks, including early diagnosis, deterioration prediction, and treatment recommendations in healthcare environments where incomplete data is a common challenge.

Future research on the interpretability of the CSAI imputation process could further enhance its applicability in clinical applications. Furthermore, the open-source nature of CSAI encourages ongoing collaboration and iterative improvements from the research community, which is crucial to advance the field and ensure its broader adoption in medical data analysis.

Despite these promising results, there are areas where CSAI’s performance indicates room for improvement. In the MIMIC_89f dataset, CSAI slightly underperformed compared to the baseline, highlighting potential limitations in handling datasets with a higher proportion of categorical variables. This suggests a need for further refinement in the integration of domain-specific knowledge into the model and additional exploration of training data strategies to improve its robustness.

Future work should also explore incorporating more granular medical knowledge, improving the model’s ability to capture long-range temporal dependencies, and developing new methods for handling extreme data sparsity. Addressing these challenges could help CSAI achieve even better performance in various healthcare datasets with distinct characteristics and missing data patterns.

The potential applications of CSAI in medical data analysis and decision making are numerous. CSAI could enhance early detection of critical conditions like sepsis and cardiac arrest by providing more accurate imputations of incomplete patient records in real time. In addition, it could help improve prediction and treatment recommendations by effectively handling missing data from various data sources from patients. As CSAI continues to evolve, it holds promise of significantly contributing to more accurate and data-driven medical decision making and improved patient outcomes.

7 Acknowledgments

This paper represents independent research funded by the NIHR Maudsley Biomedical Research Centre at South London and Maudsley NHS Foundation Trust, the EPSRC Centre for Doctoral Training in Data-Driven Health (DRIVE-Health) and King’s College London. The work of LQ is supported by the Kings-China Scholarship Council PhD Scholarship Programme (K-CSC) under Grant CSC202008060096. ZI is supported by Innovate UK under grant 10104845. TW is supported by the NIHR Maudsley Biomedical Research Centre at South London, Maudsley Charity and Early

Career Research Award from the Institute of Psychiatry, Psychology & Neuroscience. ZI and RD were supported by in part by the NIHR Biomedical Research Centre at SLaM, in part by Kings College London, London, U.K., and in part by the NIHR University College London Hospitals Biomedical Research Centre. H.L.E is supported by a Research Fellowship Award from the Department of Medicine at Dalhousie University and DRIVE-Health. All experiments are implemented on CREATE HPC (King’s College London. (2022). King’s Computational Research, Engineering and Technology Environment (CREATE)).

8 Data availability

The datasets generated and/or analysed during the current study are available from the corresponding authors on reasonable request.

9 Ethics declarations

9.1 Conflict of Interests

The authors declare that they have no conflict of interest with respect to the publication of this paper.

References

- [1] al, J.R.: Deep learning for electronic health records: A comparative review of multiple deep neural architectures. *Journal of Biomedical Informatics* **101**, 103337 (2020)
- [2] Ibrahim, Z.M., Bean, D., Searle, T., Qian, L., Wu, H., Shek, A., Kraljevic, Z., Galloway, J., Norton, S., Teo, J.T.H., Dobson, R.J.: A knowledge distillation ensemble framework for predicting short- and long-term hospitalization outcomes from electronic health records data. *IEEE Journal of Biomedical and Health Informatics* **26**(1), 423–435 (2022)
- [3] Shamout, F.E., Zhu, T., Sharma, P., Watkinson, P.J., Clifton, D.A.: Deep interpretable early warning system for the detection of clinical deterioration. *IEEE Journal of Biomedical and Health Informatics* **24**(2), 437–446 (2020)
- [4] al., R.H.: Relationship between blood pressure and incident chronic kidney disease in hypertensive patients. *Clinical Journal of the American Society of Nephrologists* **6**(11) (2011)
- [5] Wells, B.J., Chagin, K.M., Nowacki, A.S., Kattan, M.W.: Strategies for handling missing data in electronic health record derived data. *Egems* **1**(3) (2013)
- [6] Yadav, P., Steinbach, M., Kumar, V., Simon, G.: Mining electronic health records (ehrs) a survey. *ACM Computing Surveys (CSUR)* **50**(6), 1–40 (2018)

- [7] Jensen, P.B., Jensen, L.J., Brunak, S.: Mining electronic health records: towards better research applications and clinical care. *Nature Reviews Genetics* **13**(6), 395–405 (2012)
- [8] al., T.E.: A survey on missing data in machine learning. *Journal of Big Data* **8**, 140 (2021)
- [9] Zhen, H., Genevieve, M., Elliot, A., Yan, W., Mary, K., Gyorg, S.: Strategies for handling missing clinical data for automated surgical site infection detection from the electronic health record. *Journal of biomedical informatics* **68**, 112–120 (2017)
- [10] Che, Z., Purushotham, S., Cho, K., Sontag, D., Liu, Y.: Recurrent neural networks for multivariate time series with missing values. *Scientific reports* **8**(1), 1–12 (2018)
- [11] Cao, W., Wang, D., Li, J., Zhou, H., Li, L., Li, Y.: Brits: Bidirectional recurrent imputation for time series. *Advances in neural information processing systems* **31** (2018)
- [12] Yoon, J., Zame, W.R., Schaar, M.: Multi-directional recurrent neural networks: A novel method for estimating missing data. In: *Time Series Workshop in International Conference on Machine Learning* (2017)
- [13] Wang, J., Du, W., Cao, W., Zhang, K., Wang, W., Liang, Y., Wen, Q.: Deep learning for multivariate time series imputation: A survey. *arXiv preprint arXiv:2402.04059* (2024)
- [14] Fang, C., Wang, C.: Time series data imputation: A survey on deep learning approaches. *arXiv preprint arXiv:2011.11347* (2020)
- [15] al, Z.S.: Self-supervised learning of time series representation via diffusion process and imputation-interpolation-forecasting mask. In: *The 30th ACM SIGKDD Conference on Knowledge Discovery and Data Mining*, pp. 2560–2571 (2024)
- [16] Wen, Q., Zhou, T., Zhang, C., Chen, W., Ma, Z., Yan, J., Sun, L.: Transformers in time series: a survey. In: *Proceedings of the Thirty-Second International Joint Conference on Artificial Intelligence. IJCAI '23* (2023)
- [17] Du, W., Côté, D., Liu, Y.: Saits: Self-attention-based imputation for time series. *Expert Systems with Applications* **219**, 119619 (2023)
- [18] Shan, S., Li, Y., Oliva, J.B.: Nrtsi: Non-recurrent time series imputation. In: *ICASSP 2023 - 2023 IEEE International Conference on Acoustics, Speech and Signal Processing (ICASSP)*, pp. 1–5 (2023)

- [19] Jun, E., Mulyadi, A.W., Choi, J., Suk, H.-I.: Uncertainty-gated stochastic sequential model for ehr mortality prediction. *IEEE Transactions on Neural Networks and Learning Systems* **32**(9), 4052–4062 (2020)
- [20] Mulyadi, A.W., Jun, E., Suk, H.-I.: Uncertainty-aware variational-recurrent imputation network for clinical time series. *IEEE Transactions on Cybernetics* (2021)
- [21] Luo, Y., Cai, X., Zhang, Y., Xu, J., et al.: Multivariate time series imputation with generative adversarial networks. *Advances in neural information processing systems* **31** (2018)
- [22] Tashiro, Y., Song, J., Song, Y., Ermon, S.: Csd: Conditional score-based diffusion models for probabilistic time series imputation. *Advances in Neural Information Processing Systems* **34**, 24804–24816 (2021)
- [23] Mescheder, L., Geiger, A., Nowozin, S.: Which training methods for gans do actually converge? In: *International Conference on Machine Learning*, pp. 3481–3490 (2018). PMLR
- [24] Pollard, T.e.a.: The eicu collaborative research database, a freely available multi-center database for critical care research. *Scientific data* **5**(1), 1–13 (2018)
- [25] Sheikhalishahi, S., Balaraman, V., Osmani, V.: Benchmarking machine learning models on multi-centre eicu critical care dataset. *Plos one* **15**(7), 0235424 (2020)
- [26] Johnson, A., al.: MIMIC-III, a freely accessible critical care database. *Scientific data* **3**(1), 1–9 (2016)
- [27] Purushotham, S., Meng, C., Che, Z., Liu, Y.: Benchmarking deep learning models on large healthcare datasets. *Journal of biomedical informatics* **83**, 112–134 (2018)
- [28] Harutyunyan, H., Khachatrian, H., Kale, D.C., Ver Steeg, G., Galstyan, A.: Multitask learning and benchmarking with clinical time series data. *Scientific data* **6**(1), 96 (2019)
- [29] Silva, I., Moody, G., Scott, D., Celi, L., Mark, R.: Predicting in-hospital mortality of ICU patients: The Physionet/Computing in Cardiology Challenge 2012. *Computational Cardiology* **39**, 245–248 (2012)